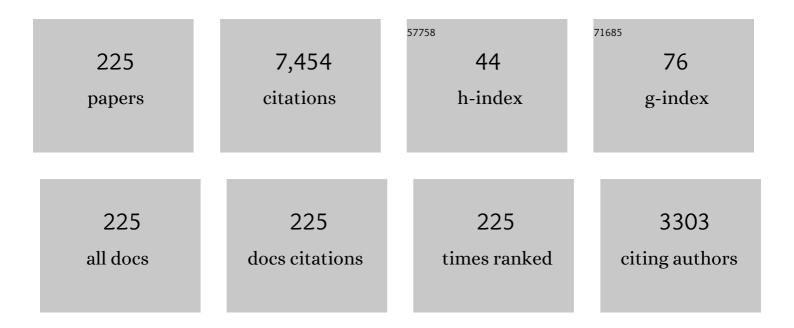
Eiji Akiyama

List of Publications by Year in descending order

Source: https://exaly.com/author-pdf/917105/publications.pdf Version: 2024-02-01



ΕΠΙ ΔΕΙΧΑΜΑ

#	Article	IF	CITATIONS
1	Realâ€Time Visualization of Hydrogen Distribution in Metals Using Polyaniline: An Ultrasensitive Hydrogenochromic Sensor. Advanced Materials Interfaces, 2022, 9, .	3.7	5
2	Effects of Thermomechanical Processing on Hydrogen Embrittlement Properties of UltraHigh-Strength TRIP-Aided Bainitic Ferrite Steels. Metals, 2022, 12, 269.	2.3	1
3	Hydrogen-accelerated fatigue crack growth of equiatomic Fe–Cr–Ni–Mn–Co high-entropy alloy evaluated by compact tension testing. Materials Science & Engineering A: Structural Materials: Properties, Microstructure and Processing, 2022, 848, 143394.	5.6	5
4	Hydrogen-assisted damage evolution in nitrogen-doped duplex stainless steel. International Journal of Hydrogen Energy, 2021, 46, 2716-2728.	7.1	7
5	Activation energy of hydrogen desorption from high-performance titanium oxide carrier-selective contacts with silicon oxide interlayers. Current Applied Physics, 2021, 21, 36-42.	2.4	12
6	Effect of Hydrogen on Spot Welded Tensile Properties in Automotive Ultrahigh Strength TRIP-aided Martensitic Steel Sheet. Tetsu-To-Hagane/Journal of the Iron and Steel Institute of Japan, 2021, 107, 175-184.	0.4	0
7	Potential Effects of Short-Range Order on Hydrogen Embrittlement of Stable Austenitic Steels—A Review. Advanced Structured Materials, 2021, , 1-18.	0.5	0
8	Effect of Carbon Content on V-Bending in High-Strength TRIP-Aided Dual-Phase Steel Sheets with Polygonal Ferrite Matrix. ISIJ International, 2021, 61, 608-616.	1.4	3
9	Hydrogen Embrittlement Behavior of Pure Ni and Ni-20Cr Alloy with Different Grain Sizes. Nippon Kinzoku Gakkaishi/Journal of the Japan Institute of Metals, 2021, 85, 49-58.	0.4	5
10	Effects of Matrix Structure and Nitrogen Content on Fatigue Properties of Ultrahigh-Strength Low Alloy TRIP-Aided Steels. ISIJ International, 2021, 61, 591-598.	1.4	2
11	Roles of Hydrogen Content and Pre-strain on Damage Evolution of TRIP-aided Bainitic Ferrite Steel. ISIJ International, 2021, 61, 1309-1314.	1.4	1
12	Effect of hydrogen charging time on hydrogen blister and hydrogen-induced cracking of pure iron. Corrosion Science, 2021, 181, 109200.	6.6	24
13	Effect of austempering treatment on the microstructure and mechanical properties of 0.4C–1.5Si-1.5Mn TRIP-aided bainitic ferrite steel. Materials Science & Engineering A: Structural Materials: Properties, Microstructure and Processing, 2021, 819, 141479.	5.6	17
14	Strain rate sensitivity of hydrogen-assisted ε-martensitic transformation and associated hydrogen embrittlement in high-Mn steel. International Journal of Hydrogen Energy, 2021, 46, 27221-27233.	7.1	13
15	Hydrogen embrittlement and associated surface crack growth in fine-grained equiatomic CoCrFeMnNi high-entropy alloys with different annealing temperatures evaluated by tensile testing under in situ hydrogen charging. International Journal of Hydrogen Energy, 2021, 46, 33028-33038.	7.1	16
16	Depressurization-induced diffusionless transformation in pure iron hydrogenated under several gigapascals. Materials Letters: X, 2021, 11, 100078.	0.7	1
17	Effects of Si and Mn Contents on V-bending in High Strength TRIP-aided Dual-Phase Steel Sheets with Polygonal Ferrite Matrix. Tetsu-To-Hagane/Journal of the Iron and Steel Institute of Japan, 2021, 107, 154-164.	0.4	2
18	V-bendability of Ultrahigh Strength Low Alloy TRIP-aided Steel Sheets with Bainitic Ferrite Matrix. Tetsu-To-Hagane/Journal of the Iron and Steel Institute of Japan, 2021, 107, 165-174.	0.4	0

#	Article	IF	CITATIONS
19	Effect of Hydrogen on Spot-Welded Tensile Properties in Automotive Ultrahigh-Strength TRIP-Aided Martensitic Steel Sheet. ISIJ International, 2021, 61, 2644-2653.	1.4	2
20	Strain rate and hydrogen effects on crack growth from a notch in a Fe-high-Mn steel containing 1.1Âwt% solute carbon. International Journal of Hydrogen Energy, 2020, 45, 1125-1139.	7.1	19
21	Effects of Alloying Elements Addition on Delayed Fracture Properties of Ultra High-Strength TRIP-Aided Martensitic Steels. Metals, 2020, 10, 6.	2.3	21
22	Quantitative Evaluation of Hydrogen Effects on Evolutions of Deformation-Induced ε-Martensite and Damage in a High-Mn Steel. Metallurgical and Materials Transactions A: Physical Metallurgy and Materials Science, 2020, 51, 6184-6194.	2.2	14
23	Role of mill scale on corrosion behavior of steel rebars in mortar. Corrosion Science, 2020, 177, 108995.	6.6	18
24	Effects of residual stress and plastic strain on hydrogen embrittlement of a stretch-formed TRIP-aided martensitic steel sheet. Corrosion Science, 2020, 177, 108957.	6.6	21
25	Pre-strain effects on critical stress and hydrogen content for hydrogen-induced quasi-cleavage fracture in a TRIP-aided bainitic ferrite steel: Martensitic transformation, matrix damage, and strain aging. International Journal of Hydrogen Energy, 2020, 45, 27920-27928.	7.1	17
26	Effects of Mn Content and Grain Size on Hydrogen Embrittlement Susceptibility of Face-Centered Cubic High-Entropy Alloys. Metallurgical and Materials Transactions A: Physical Metallurgy and Materials Science, 2020, 51, 5612-5616.	2.2	30
27	Application of an iridium complex for detecting hydrogen permeation through pure iron. International Journal of Hydrogen Energy, 2020, 45, 25580-25586.	7.1	12
28	Hydrogen Enhances Shape Memory Effect of a Ferrous Face-Centered Cubic Alloy. Metallurgical and Materials Transactions A: Physical Metallurgy and Materials Science, 2020, 51, 4439-4441.	2.2	6
29	Effects of hydrogen content that alters damage evolution mechanisms in SUH 660 precipitation-strengthened Fe–Cr–Ni steel. Materials Science & Engineering A: Structural Materials: Properties, Microstructure and Processing, 2020, 791, 139750.	5.6	4
30	Hydrogen embrittlement resistance of pre-strained ultra-high-strength low alloy TRIP-aided steel. International Journal of Fracture, 2020, 224, 253-260.	2.2	18
31	Review of Hydrogen Embrittlement in Metals: Hydrogen Diffusion, Hydrogen Characterization, Hydrogen Embrittlement Mechanism and Prevention. Acta Metallurgica Sinica (English Letters), 2020, 33, 759-773.	2.9	142
32	Multiple damage mechanisms facilitated by planar dislocation glide in a commercial-grade precipitation-strengthened Fe–Ni–Cr-based steel. Materials Science & Engineering A: Structural Materials: Properties, Microstructure and Processing, 2020, 782, 139250.	5.6	8
33	Availability of Opal Photonic Crystal Films for Visualizing Heterogeneous Strain Evolution in Steels: Example of LÃ1⁄4ders Deformation. ISIJ International, 2020, 60, 2604-2608.	1.4	7
34	Effect of Carbon Content on V-bending in High-Strength TRIP-aided Dual-Phase Steel Sheets with Polygonal Ferrite Matrix. Tetsu-To-Hagane/Journal of the Iron and Steel Institute of Japan, 2020, 106, 934-943.	0.4	4
35	Effect of Strain Rate on the Hydrogen Embrittlement Property of Ultra High-strength Low-alloy TRIP-aided Steel. Tetsu-To-Hagane/Journal of the Iron and Steel Institute of Japan, 2019, 105, 443-451.	0.4	3
36	Transformation-assisted hydrogen desorption during deformation in steels: Examples of α′- and ε-Martensite. International Journal of Hydrogen Energy, 2019, 44, 30472-30477.	7.1	23

#	Article	IF	CITATIONS
37	Detection of hydrogen effusion before, during, and after martensitic transformation: Example of multiphase transformation-induced plasticity steel. International Journal of Hydrogen Energy, 2019, 44, 26028-26035.	7.1	12
38	An Evaluation Method for Hydrogen Embrittlement of High Strength Steel Sheets Using U-bend Specimens. Tetsu-To-Hagane/Journal of the Iron and Steel Institute of Japan, 2019, 105, 927-934.	0.4	10
39	Lowering Strain Rate Simultaneously Enhances Carbon- and Hydrogen-Induced Mechanical Degradation in an Fe-33Mn-1.1C Steel. Metallurgical and Materials Transactions A: Physical Metallurgy and Materials Science, 2019, 50, 1137-1141.	2.2	12
40	Hydrogen embrittlement of high strength steam turbine last stage blade steels: Comparison between PH17-4 steel and PH13-8Mo steel. Materials Science & Engineering A: Structural Materials: Properties, Microstructure and Processing, 2019, 742, 353-363.	5.6	26
41	Hydrogen embrittlement behavior of Inconel 718 alloy at room temperature. Journal of Materials Science and Technology, 2019, 35, 499-502.	10.7	24
42	Corrosion Behavior of Reinforcing Steel with Mill Scale in Concrete. ECS Meeting Abstracts, 2019, , .	0.0	0
43	High-concentration carbon assists plasticity-driven hydrogen embrittlement in a Fe-high Mn steel with a relatively high stacking fault energy. Materials Science & Engineering A: Structural Materials: Properties, Microstructure and Processing, 2018, 717, 78-84.	5.6	18
44	Interstitial Carbon Enhanced Corrosion Resistance of Fe-33Mn-xC Austenitic Steels: Inhibition of Anodic Dissolution. Journal of the Electrochemical Society, 2018, 165, C19-C26.	2.9	16
45	Effect of Strain Rate on the Hydrogen Embrittlement Property of Ultra High-strength Low Alloy TRIP-aided Steel. ISIJ International, 2018, 58, 751-759.	1.4	32
46	Hydrogen embrittlement properties of nitrogen added ultra-high-strength TRIP-aided martensitic steels evaluated by using conventional strain rate technique. Procedia Manufacturing, 2018, 15, 1581-1587.	1.9	8
47	Tensile mechanical properties and fracture behaviors of nickel-based superalloy 718 in the presence of hydrogen. International Journal of Hydrogen Energy, 2018, 43, 20118-20132.	7.1	42
48	Corrections of the text and the figure in the paper "Effect of Strain Rate on the Hydrogen Embrittlement Property of Ultra High-strength Low Alloy TRIP-aided Steel―[ISIJ International, Vol. 58 (2018), No. 4, pp. 751–759]. ISIJ International, 2018, 58, 1748-1749.	1.4	0
49	Effects of Oxygen Pressure and Chloride Ion Concentration on Corrosion of Iron in Mortar Exposed to Pressurized Humid Oxygen Gas. Journal of the Electrochemical Society, 2018, 165, C582-C589.	2.9	17
50	Microstructural and crystallographic study of hydrogen-assisted cracking in high strength PSB1080 steel. International Journal of Hydrogen Energy, 2018, 43, 17898-17911.	7.1	38
51	Hyperbaric-Oxygen Accelerated Corrosion Test of Iron in Cement Paste and Mortar. Nippon Kinzoku Gakkaishi/Journal of the Japan Institute of Metals, 2018, 82, 1-7.	0.4	2
52	Hyperbaric-Oxygen Accelerated Corrosion Test for Iron in Cement Paste and Mortar. Materials Transactions, 2018, 59, 927-934.	1.2	10
53	Effect of Interstitial Carbon on Anodic Polarization Behavior of Fe-33Mn-C Austenitic Steels. ECS Meeting Abstracts, 2018, , .	0.0	0
54	Size and distribution of micropores and voids in 5052 aluminum alloys during tensile deformation. Keikinzoku/Journal of Japan Institute of Light Metals, 2018, 68, 630-634.	0.4	0

#	Article	IF	CITATIONS
55	Electrochemical Hydrogen Permeation Tests under Conventional Potentiostatic Hydrogen Charging Conditions Conventionally Used for Hydrogen Embrittlement Study. ECS Transactions, 2017, 75, 23-31.	0.5	10
56	Recent progress in microstructural hydrogen mapping in steels: Quantification, kinetic analysis, and multi-scale characterisation. Materials Science and Technology, 2017, 33, 1481-1496.	1.6	125
57	Hydrogen Entry into an AISI 4135 High Strength Steel in Tribocorrosion Environment. ECS Transactions, 2017, 75, 33-41.	0.5	2
58	Overview of hydrogen embrittlement in high-Mn steels. International Journal of Hydrogen Energy, 2017, 42, 12706-12723.	7.1	228
59	Effect of heat treatment on hydrogen-assisted fracture behavior of PH13-8Mo steel. Corrosion Science, 2017, 128, 198-212.	6.6	30
60	Room-temperature blue brittleness of Fe-Mn-C austenitic steels. Scripta Materialia, 2017, 141, 20-23.	5.2	37
61	Warm tempforming effect on the hydrogen embrittlement of 1.8-GPa-class ultra-high-strength low-alloy steel. Materials Science & Engineering A: Structural Materials: Properties, Microstructure and Processing, 2017, 703, 503-512.	5.6	20
62	Interfacial hydrogen localization in austenite/martensite dualâ€phase steel visualized through optimized silver decoration and scanning Kelvin probe force microscopy. Materials and Corrosion - Werkstoffe Und Korrosion, 2017, 68, 306-310.	1.5	20
63	Effects of Hydrogen on Tensile Properties at Slow Strain Rate of Ultra High-Strength TRIP-aided Bainitic Ferrite Steels. Procedia Engineering, 2017, 207, 1868-1873.	1.2	6
64	Acceleration of Fe Corrosion in Cement Paste and Mortar By Enhancing Oxygen Supply. ECS Meeting Abstracts, 2017, , .	0.0	0
65	Hydrogen Embrittlement of Metallic Materials and Recent Subjects. Materia Japan, 2017, 56, 230-233.	0.1	3
66	Electrochemical Hydrogen Permeation Test under Controlled Temperature and Humidity after Outdoor Exposure at Beijing, Chongqing and Okinawa. Tetsu-To-Hagane/Journal of the Iron and Steel Institute of Japan, 2017, 103, 93-100.	0.4	0
67	Comparison of Constant Load, SSRT and CSRT Methods for Hydrogen Embrittlement Evaluation Using Round Bar Specimens of High Strength Steels. ISIJ International, 2016, 56, 1268-1275.	1.4	32
68	Electrochemical Hydrogen Permeation Test under Controlled Temperature and Humidity after Outdoor Exposure at Beijing, Chongqing and Okinawa. ISIJ International, 2016, 56, 436-443.	1.4	9
69	Martensitic transformation-induced hydrogen desorption characterized by utilizing cryogenic thermal desorption spectroscopy during cooling. Scripta Materialia, 2016, 122, 50-53.	5.2	34
70	Hydrogen-assisted damage in austenite/martensite dual-phase steel. Philosophical Magazine Letters, 2016, 96, 9-18.	1.2	25
71	Electrochemical hydrogen permeation tests under galvanostatic hydrogen charging conditions conventionally used for hydrogen embrittlement study. Corrosion Reviews, 2016, 34, 103-112.	2.0	29
72	Electrochemical Hydrogen Permeation Tests Under Potentiostatic Hydrogen Charging Conditions Conventionally Used for Hydrogen Embrittlement Study. ECS Meeting Abstracts, 2016, , .	0.0	1

#	Article	IF	CITATIONS
73	Hydrogen Entry into an AISI 4135 High Strength Steel in Tribocorrosion Environment. ECS Meeting Abstracts, 2016, , .	0.0	0
74	Hydrogen Visualization in Steels Using Ag Decoration Method. Materials Transactions, 2015, 56, 793-797.	1.2	21
75	Spatially and Kinetically Resolved Mapping of Hydrogen in a Twinning-Induced Plasticity Steel by Use of Scanning Kelvin Probe Force Microscopy. Journal of the Electrochemical Society, 2015, 162, C638-C647.	2.9	64
76	Comparison of Constant Load, SSRT and CSRT Methods for Hydrogen Embrittlement Evaluation Using Round Bar Specimens of High Strength Steels. Tetsu-To-Hagane/Journal of the Iron and Steel Institute of Japan, 2014, 100, 1298-1305.	0.4	23
77	Hydrogen Thermal Desorption Analysis for the Studies of Hydrogen Embrittlement of High Strength Steels. Journal of the Vacuum Society of Japan, 2014, 57, 207-213.	0.3	7
78	Hydrogen Embrittlement in Al-Added Twinning-Induced Plasticity Steels Evaluated by Tensile Tests during Hydrogen Charging. Tetsu-To-Hagane/Journal of the Iron and Steel Institute of Japan, 2014, 100, 662-667.	0.4	0
79	Factors Affecting Static Strain Aging Under Stress at Room Temperature in a Fe-Mn-C Twinning-Induced Plasticity Steel. Tetsu-To-Hagane/Journal of the Iron and Steel Institute of Japan, 2014, 100, 1123-1131.	0.4	2
80	Hydrogen-assisted decohesion and localized plasticity in dual-phase steel. Acta Materialia, 2014, 70, 174-187.	7.9	366
81	Hydrogen embrittlement associated with strain localization in a precipitation-hardened Fe–Mn–Al–C light weight austenitic steel. International Journal of Hydrogen Energy, 2014, 39, 4634-4646.	7.1	170
82	Effects of Static and Dynamic Strain Aging on Hydrogen Embrittlement in TWIP Steels Containing Al. Tetsu-To-Hagane/Journal of the Iron and Steel Institute of Japan, 2014, 100, 1132-1139.	0.4	5
83	Hydrogen-assisted quasi-cleavage fracture in a single crystalline type 316 austenitic stainless steel. Corrosion Science, 2013, 75, 345-353.	6.6	85
84	The Use of Renewable Energy in the Form of Methane Via Electrolytic Hydrogen Generation / Zastosowanie Odnawialnej Energii W Formie Metanu Na Drodze Elektrolitycznej Produkcji Wodoru. Archives of Metallurgy and Materials, 2013, 58, 231-239.	0.6	8
85	Studies of Evaluation of Hydrogen Embrittlement Property of High-Strength Steels with Consideration of the Effect of Atmospheric Corrosion. Metallurgical and Materials Transactions A: Physical Metallurgy and Materials Science, 2013, 44, 1290-1300.	2.2	43
86	Hydrogen-assisted failure in a twinning-induced plasticity steel studied under in situ hydrogen charging by electron channeling contrast imaging. Acta Materialia, 2013, 61, 4607-4618.	7.9	218
87	Fretting fatigue behaviour of Ni-free high-nitrogen stainless steel in a simulated body fluid. Science and Technology of Advanced Materials, 2013, 14, 025002.	6.1	14
88	Hydrogen Visualization in Steels Using Ag Decoration Method. Nippon Kinzoku Gakkaishi/Journal of the Japan Institute of Metals, 2013, 77, 622-626.	0.4	8
89	Factors Affecting Static Strain Aging under Stress at Room Temperature in a Fe–Mn–C Twinning-induced Plasticity Steel. ISIJ International, 2013, 53, 1089-1096.	1.4	9
90	Effects of Static and Dynamic Strain Aging on Hydrogen Embrittlement in TWIP Steels Containing Al. ISIJ International, 2013, 53, 1268-1274.	1.4	24

#	Article	IF	CITATIONS
91	Hydrogen Entry Behavior into Iron and Steel under Atmospheric Corrosion. ISIJ International, 2013, 53, 1062-1069.	1.4	18
92	Hydrogen Entry Behavior into Iron and Steels under Atmospheric Corrosion. Tetsu-To-Hagane/Journal of the Iron and Steel Institute of Japan, 2013, 99, 651-658.	0.4	5
93	Hydrogen Embrittlement in Al-added Twinning-induced Plasticity Steels Evaluated by Tensile Tests during Hydrogen Charging. ISIJ International, 2012, 52, 2283-2287.	1.4	35
94	Hydrogen embrittlement in a Fe–Mn–C ternary twinning-induced plasticity steel. Corrosion Science, 2012, 54, 1-4.	6.6	134
95	Effect of hydrogen content on the embrittlement in a Fe–Mn–C twinning-induced plasticity steel. Corrosion Science, 2012, 59, 277-281.	6.6	103
96	Evaluation of Delayed Fracture Property of High Strength Bolt Steels. ISIJ International, 2012, 52, 307-315.	1.4	45
97	Hydrogen Embrittlement of a 1500-MPa Tensile Strength Level Steel with an Ultrafine Elongated Grain Structure. Metallurgical and Materials Transactions A: Physical Metallurgy and Materials Science, 2012, 43, 1670-1687.	2.2	61
98	Hydrogen-induced cracking at grain and twin boundaries in an Fe–Mn–C austenitic steel. Scripta Materialia, 2012, 66, 459-462.	5.2	168
99	Hydrogen-induced delayed fracture of a Fe–22Mn–0.6C steel pre-strained at different strain rates. Scripta Materialia, 2012, 66, 947-950.	5.2	50
100	Preface to the Special Issue on "Common Bases for Hydrogen Embrittlement Studies― ISIJ International, 2012, 52, 167.	1.4	10
101	Corrosion behaviour of sputter-deposited Mg–Zr alloys in a borate buffer solution. Corrosion Science, 2011, 53, 2988-2993.	6.6	32
102	Constant-load delayed fracture test of atmospherically corroded high strength steels. Applied Surface Science, 2011, 257, 8275-8281.	6.1	30
103	Hydrogen entry into Fe and high strength steels under simulated atmospheric corrosion. Electrochimica Acta, 2011, 56, 1799-1805.	5.2	77
104	Delayed Fracture of High Strength Steels under Atmospheric Corrosion. Zairyo To Kankyo/ Corrosion Engineering, 2011, 60, 184-189.	0.2	4
105	Hydrogen embrittlement property of a 1700-MPa-class ultrahigh-strength tempered martensitic steel. Science and Technology of Advanced Materials, 2010, 11, 025005.	6.1	51
106	Evaluation of hydrogen entry into high strength steel under atmospheric corrosion. Corrosion Science, 2010, 52, 2758-2765.	6.6	115
107	Evaluation of susceptibility of high strength steels to delayed fracture by using cyclic corrosion test and slow strain rate test. Corrosion Science, 2010, 52, 1660-1667.	6.6	69
108	Evaluation of delayed fracture property of outdoor-exposed high strength AISI 4135 steels. Corrosion Science, 2010, 52, 3198-3204.	6.6	34

#	Article	lF	CITATIONS
109	Effects of severe plastic deformation on the corrosion behavior of aluminum alloys. Journal of Solid State Electrochemistry, 2009, 13, 277-282.	2.5	55
110	Evaluation of Delayed Fracture Characteristics of High Strength Steel based on CSRT Method. Tetsu-To-Hagane/Journal of the Iron and Steel Institute of Japan, 2008, 94, 215-221.	0.4	70
111	The role of corrosion-resistant alloying elements in passivity. Corrosion Science, 2007, 49, 42-52.	6.6	137
112	Effect of α-Al/Al3Ni microstructure on the corrosion behaviour of Al–5.4wt% Ni alloy fabricated by equal-channel angular pressing. Corrosion Science, 2007, 49, 2962-2972.	6.6	47
113	Effect of hydrogen on the fracture behavior of high strength steel during slow strain rate test. Corrosion Science, 2007, 49, 4081-4097.	6.6	336
114	Determination of the critical hydrogen concentration for delayed fracture of high strength steel by constant load test and numerical calculation. Corrosion Science, 2006, 48, 2189-2202.	6.6	129
115	Discrete electrochemical transients of aluminium alloys generated by slurry jet impingement. Journal Physics D: Applied Physics, 2006, 39, 3157-3164.	2.8	11
116	Fracture criterion for hydrogen embrittlement of high strength steel. Materials Science and Technology, 2006, 22, 167-172.	1.6	40
117	Acetate and Chloride Effects on Hydrogen Production across Crevices. Materials Science Forum, 2006, 512, 97-102.	0.3	1
118	Effect of Hydrogen on the Fracture Behavior of High-Strength Cr-Mo Steel. Materials Science Forum, 2006, 512, 55-60.	0.3	6
119	Depassivation and Repassivation of Titanium under Particle Impingements. ECS Transactions, 2006, 1, 437-446.	0.5	8
120	Hydrogen Entry in Crevice Region: Evaluation by Hydrogen Permeation Technique. ISIJ International, 2006, 46, 1081-1085.	1.4	8
121	Hydrogen degradation of a boron-bearing steel with 1050 and 1300MPa strength levels. Scripta Materialia, 2005, 52, 403-408.	5.2	130
122	Crosshead speed dependence of the notch tensile strength of a high strength steel in the presence of hydrogen. Scripta Materialia, 2005, 53, 713-718.	5.2	99
123	Hydrogen mapping across a crevice: Effect of applied potential. Scripta Materialia, 2005, 53, 1219-1223.	5.2	14
124	Effect of hydrogen and stress concentration on the notch tensile strength of AISI 4135 steel. Materials Science & Engineering A: Structural Materials: Properties, Microstructure and Processing, 2005, 398, 37-46.	5.6	226
125	Hydrogen Mapping Across Crevices. Electrochemical and Solid-State Letters, 2005, 8, B30.	2.2	12
126	Storage and Release of Soluble Hexavalent Chromium from Chromate Conversion Coatings on Al Alloys: Kinetics of Release. Journal of the Electrochemical Society, 2003, 150, B83.	2.9	46

#	Article	IF	CITATIONS
127	Materials for global carbon dioxide recycling. Corrosion Science, 2002, 44, 371-386.	6.6	55
128	Distribution of Hydrogen Occluded in Bolts Tightened beyond the Yield Strength and Exposed at a Seashore Site. Tetsu-To-Hagane/Journal of the Iron and Steel Institute of Japan, 2002, 88, 849-856.	0.4	19
129	Advanced materials for global carbon dioxide recycling. Materials Science & Engineering A: Structural Materials: Properties, Microstructure and Processing, 2001, 304-306, 88-96.	5.6	54
130	Angle-resolved XPS for determination of diffusion coefficients and mobilities of cations in thin passive films. Surface and Interface Analysis, 2000, 30, 106-111.	1.8	4
131	XPS Determination of Diffusion Coefficients of Cations in Thin Passive Films on Alloys. Solid State Phenomena, 2000, 72, 79-84.	0.3	1
132	Effects of nanocrystalline heterogeneity on the corrosion behavior of sputter-deposited chromium–niobium alloys. Corrosion Science, 2000, 42, 361-382.	6.6	16
133	Storage and Release of Soluble Hexavalent Chromium from Chromate Conversion Coatings Equilibrium Aspects of Cr[sup VI] Concentration. Journal of the Electrochemical Society, 2000, 147, 2556.	2.9	177
134	Global CO2 recycling—novel materials and prospect for prevention of global warming and abundant energy supply. Materials Science & Engineering A: Structural Materials: Properties, Microstructure and Processing, 1999, 267, 200-206.	5.6	99
135	CO2 methanation catalysts prepared from amorphous Ni–Zr–Sm and Ni–Zr–misch metal alloy precursors. Materials Science & Engineering A: Structural Materials: Properties, Microstructure and Processing, 1999, 267, 220-226.	5.6	57
136	Oxygen evolution on manganese–molybdenum oxide anodes in seawater electrolysis. Materials Science & Engineering A: Structural Materials: Properties, Microstructure and Processing, 1999, 267, 254-259.	5.6	65
137	The sulfidation and oxidation behavior of sputter-deposited Alî—,Nbî—,Mo alloys. Materials Science & Engineering A: Structural Materials: Properties, Microstructure and Processing, 1999, 267, 277-284.	5.6	1
138	Corrosion-resistant Mnî—,Zrî—,Cr alloys in chloride-containing media. Materials Science & Engineering A: Structural Materials: Properties, Microstructure and Processing, 1999, 267, 285-293.	5.6	6
139	Title is missing!. Journal of Applied Electrochemistry, 1999, 29, 769-775.	2.9	74
140	The Influence of Dichromate Ions on Aluminum Dissolution Kinetics in Artificial Crevice Electrode Cells. Journal of the Electrochemical Society, 1999, 146, 4095-4100.	2.9	35
141	Electrochemical and XPS studies of the corrosion behavior of sputter-deposited amorphous Fe–Cr–Ni–Nb alloys in 6 M HCl. Corrosion Science, 1999, 41, 1095-1118.	6.6	11
142	The corrosion behavior of sputter-deposited amorphous Fe–Cr–Ni–Ta alloys in 12 M HCl. Corrosion Science, 1999, 41, 1849-1869.	6.6	21
143	The degradation of the corrosion resistance of sputter-deposited chromium–titanium alloys by nanoscale heterogeneity. Corrosion Science, 1999, 41, 1871-1890.	6.6	23
144	Anodically deposited manganese oxide and manganese–tungsten oxide electrodes for oxygen evolution from seawater. Electrochimica Acta, 1998, 43, 3303-3312.	5.2	96

#	Article	lF	CITATIONS
145	Electrochemical and XPS studies on the passivation behavior of sputter-deposited W-Cr Alloys in 12 M HCl solution. Corrosion Science, 1998, 40, 155-175.	6.6	31
146	Experimental evidence for the critical size of heterogeneity areas for pitting corrosion of Cr-Zr alloys in 6 M HCl. Corrosion Science, 1998, 40, 1-17.	6.6	68
147	Electrochemical and XPS studies of the corrosion behavior of sputter-deposited W-Nb alloys in concentrated hydrochloric acid solutions. Corrosion Science, 1998, 40, 19-42.	6.6	32
148	Passivity and its breakdown on sputter-deposited amorphous Mn-Zr alloys in neutral chloride solutions. Corrosion Science, 1998, 40, 235-250.	6.6	6
149	The passivation behavior of sputter-deposited W-Ta alloys in 12 M HCl. Corrosion Science, 1998, 40, 757-779.	6.6	53
150	An XPS study of passive films on sputter-deposited Cr-Nb alloys in 12 M HCl solution. Corrosion Science, 1998, 40, 821-838.	6.6	18
151	The effect of alloying elements on the corrosion behaviour of sputter-deposited amorphous Mn–Ta–Cr alloys in 1 M H2SO4. Corrosion Science, 1998, 40, 1491-1512.	6.6	11
152	XPS and electrochemical studies on the corrosion behaviour of sputter-deposited amorphous Mn-Nb alloys in a neutral chloride solution. Corrosion Science, 1998, 40, 1513-1531.	6.6	17
153	Electrochemical and XPS studies of the passivation behavior of sputter-deposited Cr–Ta alloys in 12 M HCl. Corrosion Science, 1998, 40, 1587-1604.	6.6	14
154	The influence of concentration of hydrochloric acid solutions on the passivation behavior of sputter-deposited tungsten rich W–Nb alloys. Corrosion Science, 1998, 40, 1897-1914.	6.6	9
155	The effect of heat treatment on the corrosion behavior of sputter-deposited aluminum–chromium alloys. Corrosion Science, 1998, 41, 477-499.	6.6	38
156	Characterization of CO2 methanation catalysts prepared from amorphous Ni-Zr and NI-Zr-rare earth element alloys. Studies in Surface Science and Catalysis, 1998, 114, 451-454.	1.5	14
157	Hydrogen Evolution Characteristics of Sputter-Deposited Co–Mo, Co–Al and Co–Mo–Al Alloy Electrodes in NaOH Solution. Materials Transactions, JIM, 1998, 39, 1017-1023.	0.9	5
158	Mn–W Oxide Anodes Prepared by Thermal Decomposition for Oxygen Evolution in Seawater Electrolysis. Materials Transactions, JIM, 1998, 39, 308-313.	0.9	15
159	The Corrosion Behavior of Ni-Cr-Mo Ternary Alloys in Hot Concentrated Sulfuric Acids with Active Carbon (Part 1). Zairyo To Kankyo/ Corrosion Engineering, 1997, 46, 643-650.	0.2	2
160	The Microcomposite Structure of Catalysts Prepared by Oxidation of Amorphous Ni–Ta–Pd Alloys. Materials Transactions, JIM, 1997, 38, 123-132.	0.9	0
161	Effects of Additional Elements on Electrocatalytic Properties of Thermally Decomposed Manganese Oxide Electrodes for Oxygen Evolution from Seawater. Materials Transactions, JIM, 1997, 38, 899-905.	0.9	34
162	Application of Sputter Deposition Technique to the Preparation of Amorphous Alloy-Derived Catalysts for NO Decomposition. Materials Transactions, JIM, 1997, 38, 643-649.	0.9	0

#	Article	IF	CITATIONS
163	The corrosion behaviour of sputter-deposited amorphous Mn-Ti alloys in 0.5 M NaCl solutions. Corrosion Science, 1997, 39, 305-320.	6.6	29
164	The roles of tantalum and phosphorus in the corrosion behavior of Ni-Ta-P alloys in 12 M HCl. Corrosion Science, 1997, 39, 321-332.	6.6	18
165	The effect of molybdenum on the stability of passive films formed on amorphous Fe-Cr-Mo-P-C alloys by potentiostatic polarization in deaerated 1 M HCl. Corrosion Science, 1997, 39, 589-603.	6.6	11
166	An angle-resolved xps study of the in-depth structure of passivated amorphous aluminum alloys. Corrosion Science, 1997, 39, 1351-1364.	6.6	13
167	An XPS study of passive films on corrosion-resistant Crî—,Zr alloys prepared by sputter deposition. Corrosion Science, 1997, 39, 1365-1380.	6.6	41
168	The corrosion behaviour of sputter-deposited amorphous Mn-Ta alloys in 0.5 M NaCl solution. Corrosion Science, 1997, 39, 1965-1979.	6.6	17
169	Spontaneously passivated films on sputter-deposited Cr-Ti alloys in 6 M HCl solution. Corrosion Science, 1997, 39, 935-948.	6.6	27
170	Electrochemical and xps studies of the corrosion behavior of sputter-deposited amorphous W-Zr alloys in 6 and 12 M HCl solutions. Corrosion Science, 1997, 39, 355-375.	6.6	37
171	The Corrosion Behavior of Ni-Cr-Mo Ternary Alloys in Hot Concentrated Sulfuric Acids with Active Carbon (Part 2). Zairyo To Kankyo/ Corrosion Engineering, 1997, 46, 702-708.	0.2	0
172	NO decomposition catalysts prepared from amorphous NiTaPd alloys. Applied Catalysis B: Environmental, 1997, 11, 243-255.	20.2	2
173	Surface activation of manganese oxide electrode for oxygen evolution from seawater. Journal of Applied Electrochemistry, 1997, 27, 1362-1368.	2.9	31
174	Compositional dependence of the CO2 methanation activity of Ni/ZrO2 catalysts prepared from amorphous NiZr alloy precursors. Applied Catalysis A: General, 1997, 163, 187-197.	4.3	61
175	The sulfidation and oxidation behavior of sputter-deposited Cr-refractory metal alloys at high temperatures. Materials Science & Engineering A: Structural Materials: Properties, Microstructure and Processing, 1997, 226-228, 910-914.	5.6	6
176	Corrosion-resistant amorphous aluminum alloys and structure of passive films. Materials Science & Engineering A: Structural Materials: Properties, Microstructure and Processing, 1997, 226-228, 920-924.	5.6	16
177	Characterization of sputter-deposited Ni-Mo and Ni-W alloy electrocatalysts for hydrogen evolution in alkaline solution. Materials Science & Engineering A: Structural Materials: Properties, Microstructure and Processing, 1997, 226-228, 905-909.	5.6	67
178	The corrosion behavior of amorphous and crystalline Ni-10Ta-20P alloys in 12 M HCl. Corrosion Science, 1996, 38, 1269-1279.	6.6	26
179	The effects of alloying elements on the passivity of sputter-deposited amorphous Al-Cr-Mo alloys in 1M HCl. Corrosion Science, 1996, 38, 1281-1294.	6.6	21
180	The influence of pre-immersion on the potentiostatic polarization behavior of amorphous Fe-Cr-Mo-P-C alloys in de-aerated 1 M HCl. Corrosion Science, 1996, 38, 1495-1511.	6.6	6

#	Article	IF	CITATIONS
181	The corrosion behavior of sputter-deposited amorphous Alî—,Crî—,Mo alloys in 1 M HCl. Corrosion Science, 1996, 38, 279-292.	6.6	29
182	The influences of Mo addition and air exposure on the corrosion behavior of amorphous Feî—,8Crî—,13Pî—,7C alloy in de-aerated 1 M HCl. Corrosion Science, 1996, 38, 349-365.	6.6	27
183	The corrosion behavior of sputter-deposited Moî—,Ta alloys in 12 M HCl solution. Corrosion Science, 1996, 38, 397-411.	6.6	39
184	The effect of phosphorus addition on the corrosion behavior of ARC-MELTED Niî—,10Taî—,P alloys in 12 M HCl. Corrosion Science, 1996, 38, 469-485.	6.6	6
185	A study of the structure of a passive film using angle-resolved X-ray photo-electron spectroscopy. Corrosion Science, 1996, 38, 1127-1140.	6.6	21
186	The corrosion behavior of sputter-deposited Mo-Ti alloys in concentrated hydrochloric acid. Corrosion Science, 1996, 38, 1649-1667.	6.6	51
187	The corrosion behavior of sputter-deposited Mo-Nb alloys in 12 M HCl solution. Corrosion Science, 1996, 38, 1731-1750.	6.6	34
188	The role of chromium and molybdenum in passivation of amorphous Fe-Cr-Mo-P-C alloys in deaerated 1 M HCl. Corrosion Science, 1996, 38, 2137-2151.	6.6	53
189	Global CO2 Recycling. Zairyo To Kankyo/ Corrosion Engineering, 1996, 45, 614-620.	0.2	16
190	XPS Study of Ni-Mo-B Amorphous Ultra-fine Particles Prepared by Chemical Reduction. Nippon Kinzoku Gakkaishi/Journal of the Japan Institute of Metals, 1996, 60, 79-83.	0.4	1
191	High Temperature Sulfidation and Oxidation Behavior of Sputter-Deposited Al-refractory Metal Alloys. Materials Transactions, JIM, 1996, 37, 379-382.	0.9	14
192	The Corrosion Behavior of Ni–Ta–5P Alloys in Concentrated Hydrochloric Acid. Materials Transactions, JIM, 1996, 37, 383-388.	0.9	5
193	Decomposition of nitrogen monoxide over NiTa2O6-supported palladium catalysts prepared from amorphous alloy precursors. Applied Catalysis B: Environmental, 1996, 9, 93-106.	20.2	10
194	Total Synthesis and Absolute Configuration of (-)-Sedacryptine. Synlett, 1996, 1996, 100-102.	1.8	18
195	Decomposition of nitrogen monoxide over NiTa2O6-supported palladium catalysts prepared from amorphous alloy precursors. Applied Catalysis B: Environmental, 1996, 9, 93-106.	20.2	0
196	Effect of cathodic reduction on catalytic activity of amorphous alloy electrodes for electrooxidation of sulfite. Journal of Applied Electrochemistry, 1995, 25, 953.	2.9	0
197	Recent progress in corrosion-resistant metastable alloys. Materials Science & Engineering A: Structural Materials: Properties, Microstructure and Processing, 1995, 198, 1-10.	5.6	57
198	The corrosion behavior of sputter-deposited amorphous Mo-Zr alloys in 12 M HCl. Corrosion Science, 1995, 37, 307-320.	6.6	43

#	Article	IF	CITATIONS
199	The effect of phosphorus addition on the corrosion behavior of amorphous Ni-30Ta-P alloys in 12 M HCl. Corrosion Science, 1995, 37, 321-330.	6.6	16
200	Change in the surface composition of amorphous Feî—,Crî—,Moî—,Pî—,C alloys during air exposure. Corrosion Science, 1995, 37, 331-341.	6.6	14
201	The effect of air exposure on the corrosion behavior of amorphous Fe-8Cr-Mo-13P-7C alloys in 1 M HCl. Corrosion Science, 1995, 37, 1289-1301.	6.6	67
202	The effect of microcrystallites in the amorphous matrix on the corrosion behavior of amorphous Fe-8Cr-P alloys. Corrosion Science, 1995, 37, 1411-1422.	6.6	5
203	The effect of phosphorus on the passivation behavior of Ni-10Ta-P alloys in 12 M HCl. Corrosion Science, 1995, 37, 1313-1324.	6.6	11
204	The corrosion behavior of sputter-deposited Cr-Mo alloys in 12 M HCl solution. Corrosion Science, 1995, 37, 1843-1860.	6.6	33
205	The corrosion behavior of sputter-deposited amorphous Wî—,Ti alloys in 6 M HCl solution. Corrosion Science, 1995, 37, 2071-2086.	6.6	39
206	The effect of phosphorus addition on the corrosion behavior of amorphous Fe-8Cr-P alloys in 9M H2SO4. Corrosion Science, 1995, 37, 709-722.	6.6	15
207	Preparation of Protective Multilayer SiO2 and Al2O3 Coatings on Austenitic Stainless Steel by Sol-Gel Method. Zairyo To Kankyo/ Corrosion Engineering, 1994, 43, 654-659.	0.2	7
208	Amorphous alloy electrodes for anodic oxidation of sulfite. Materials Science & Engineering A: Structural Materials: Properties, Microstructure and Processing, 1994, 181-182, 1081-1084.	5.6	2
209	Highly corrosion-resistant amorphous Crî—,Niî—,P alloys. Materials Science & Engineering A: Structural Materials: Properties, Microstructure and Processing, 1994, 181-182, 1114-1118.	5.6	5
210	Amorphous alloy catalysts for decomposition of CCl2F2 by hydrolysis. Materials Science & Engineering A: Structural Materials: Properties, Microstructure and Processing, 1994, 181-182, 1091-1094.	5.6	6
211	Effect of phosphorus on the passivation behavior of amorphous Feî—,8Crî—,13Pî—,7C alloy in 9M H2SO4 solution. Materials Science & Engineering A: Structural Materials: Properties, Microstructure and Processing, 1994, 181-182, 1119-1122.	5.6	2
212	Nitrogen monoxide decomposition catalysts prepared from amorphous Ni-valve metal-Pd alloys. Materials Science & Engineering A: Structural Materials: Properties, Microstructure and Processing, 1994, 181-182, 1123-1127.	5.6	10
213	The corrosion behaviour of sputter-deposited amorphous Niî—,Ti alloys in 1 M HCl. Materials Science & Engineering A: Structural Materials: Properties, Microstructure and Processing, 1994, 181-182, 1128-1132.	5.6	21
214	Amorphous Fe-valve metal-Pt group metal alloy catalysts for methanation of CO2. Materials Science & Engineering A: Structural Materials: Properties, Microstructure and Processing, 1994, 181-182, 1133-1136.	5.6	7
215	An XPS study of the corrosion behavior of sputter-deposited amorphous Cr-Nb and Cr-Ta alloys in 12 M HCl solution. Corrosion Science, 1994, 36, 511-523.	6.6	38
216	The corrosion behavior of amorphous Fe-8Cr-13P-7C and Fe-8Cr-20P alloys in concentrated sulfuric acid. Corrosion Science, 1994, 36, 1537-1550.	6.6	16

#	Article	IF	CITATIONS
217	The corrosion behavior of sputter-deposited amorphous Cr-Ni-Mo alloys in 12 M HCl. Corrosion Science, 1994, 36, 1395-1410.	6.6	30
218	The corrosion behavior of sputter-deposited amorphous chromium-zirconium alloys in 6 M HCl solution. Corrosion Science, 1993, 34, 1817-1827.	6.6	53
219	Electrochemical and XPS studies of the effects of alloying elements on the corrosion behavior of amorphous Feî—,Crî—,Metalloid alloys in 9 M H2SO4. Corrosion Science, 1993, 34, 1829-1839.	6.6	16
220	The corrosion behavior of sputter-deposited amorphous Crî—,Nb and Crî—,Ta alloys in 12 M HCl solution. Corrosion Science, 1993, 34, 1947-1955.	6.6	46
221	The corrosion behavior of sputter-deposited amorphous titanium-chromium alloys in 1 M and 6 M HCl solutions. Corrosion Science, 1993, 34, 975-987.	6.6	55
222	Corrosion-resistant amorphous surface alloys. Corrosion Science, 1993, 35, 363-370.	6.6	40
223	The effect of magnesium on the corrosion behavior of sputter-deposited amorphous Alî—,Mgî—,Ti ternary alloys in a neutral chloride solution. Corrosion Science, 1993, 34, 27-40.	6.6	14
224	Decomposition of Nitrogen Monoxide over Amorphous Co–65Zr Alloys Containing Platinum Group Elements. Materials Transactions, JIM, 1993, 34, 725-731.	0.9	5
225	Preparation of Protective Alumina Coating on Austenitic Stainless Steel by Sol-Gel Method. Zairyo To Kankyo/ Corrosion Engineering, 1993, 42, 158-165.	0.2	3